Journal of Solid State Chemistry 184 (2011) 1735–1739

Contents lists available at ScienceDirect

Journal of Solid State Chemistry

journal homepage: www.elsevier.com/locate/jssc

Growth of single crystalline dendritic Li_2SiO_3 arrays from $LiNO_3$ and mesoporous SiO_2

José M. Córdoba*, Mohamed A. Ballem, Emma M. Johansson, Magnus Odén

Nanostructured Materials, Department of Physics, Chemistry and Biology (IFM), Linköping University, SE-581 83 Linköping, Sweden

ARTICLE INFO

Article history:
Received 17 January 2011
Received in revised form
27 April 2011
Accepted 1 May 2011
Available online 7 May 2011

Keywords:
Solid state synthesis
Li_3SiO_4
Nanodendrite
Mesoporous silica
Mesoreactor

ABSTRACT

A solution based wet chemistry approach has been developed for synthesizing Li_2SiO_3 using $LiNO_3$ and mesoporous silica as starting materials at 550 °C. A reaction path where NO and O_2 are formed as side-products is proposed. The crystals synthesized exhibit dendritic growth where the as-prepared nanodendrite is a typical 1-fold nanodendrite composed of one several microns long and some tenth of nanometers wide trunk with small branches, which are several hundreds of nanometers long and up to 70 nm in diameter. The effect of the structure of the mesoporous silica for the final morphology is discussed.

1. Introduction

The architectural control of nanosized materials with well-defined morphologies is essential for successful "bottom-up" approaches toward future nano-devices [1]. The interest in nanostructures with anisotropic architecture (e.g. dendrites) is based on their capacity to have singular physico-chemical properties [2]. The formation of one- or two-dimensional nanostructures with well defined sizes, shapes, and crystallinity [3,4] are essential in the development of nanoscale devices such as electronics, solar cells, matrix reinforcement, photocatalysts, and batteries [5,6] when exploiting the properties of nanomaterials [7].

Lithium metasilicate (Li_2SiO_3) is one member of a large family of isostructural A_2BO_3 compounds. It has a polar orthorhombic symmetry (a=9.392 Å, b=5.397 Å, c=4.660 Å) in point group $mm2$ [8] and is thus of interest for piezoelectric, pyroelectric, electro-optic applications. At room temperature, the Li_2SiO_3 structure is in space group $Cmc21$ with (Si_2O_6) groups as chains running parallel to the polar c axis and linked together by the small lithium ions [9].

Lithium silicate are commonly used in gas barrier, sensors and as new-dielectric barrier devices [10–12], however, there is a general agreement that lithium metasilicate (and in general lithium ceramics) are the best promising material for tritium production and release through $^6Li(n_t, \alpha)^3H$ reaction [13]. These two properties determine the possible application of a tritium breeder material for fusion reactors [14] as well as its good thermal, chemical, and mechanical stability at high temperatures in combination with its favorable irradiation behavior [15]. Furthermore, it is compatible with other blanket and structural materials [14,16]. Lithium silicates have shown that control of the microstructure must be exercised when preparing this ceramic, as the microstructure may determine the rate of tritium release from the blanket [17,18] as well as dendritic inclusion in matrix has shown an improvement on the final mechanical properties of the material [18].

Different techniques have been used to synthesize the lithium silicates compounds, e.g. solid state reaction, precipitation, sol–gel method, extrusion–spherodisation process, rotating melting procedures, and combustion [19–21] resulting in non-oriented compounds. However the number of reports where oriented lithium silicates are synthesized are limited [22,23], with no reports on oriented lithium metasilicate.

Here we report on a route to design oriented lithium metasilicate with a nanodendrite microstructure based on a precursor, $LiNO_3$, in combination with mesoporous silica as the silica source and structure directing agent.

2. Materials and methods

Detailed descriptions of the synthesis routes of mesoporous silica SBA-15 and SBA-16 used here are given elsewhere [24,25]. Table 1 summarize a description of the mesoporous powders

* Corresponding author.
E-mail address: josga@ifm.liu.se (J.M. Córdoba).

0022-4596/$ - see front matter © 2011 Elsevier Inc. All rights reserved.
doi:10.1016/j.jssc.2011.05.003

Table 1
Properties of the mesoporus silicas used for the synthesis and the final product composition.

Sample	Silica source				Final product	
	SiO_2 mesoporous type	Pore arrangement	Pore size (nm)	Surface area (m^2/g)	Final product composition	$D_{Li_2SiO_3}$ (nm)
1	SBA-15	Hexagonal	20.0	540	Li_2SiO_3 (97) $Li_2Si_2O_5$ (3)	66
2	SBA-15	Hexagonal	5.0	699	Li_2SiO_3 (82) Li_2SiO_4 (18)	54
3	SBA-16	Cubic	7.8	822	Li_2SiO_3 (95) $Li_2Si_2O_5$ (5)	115

The numbers in the bracket show the I_x/I_t relation obtained by X-ray diffraction (XRD) patterns.

used here. For the synthesis of Li_2SiO_3 a solution of 0.2 M of $LiNO_3$ (purity $\geq$ 98.0%, puriss. p.a., ACS reagent, Fluka) was used as Li-precursor. Test tubes were filled with 50 mg of mesoporous silica (SBA-15 or SBA-16) and 5 ml of 0.2 M $LiNO_3$ solution. The test tube was then heated at 90 °C in an oil bath overnight (step 1). Subsequently the mixture was dried in air at 110 °C and calcinated in a muffle furnace at 600 °C for 5 h (step 2). The powders obtained were mortared and characterized.

The crystallinity of the sample was determined by powder x-ray diffractometry (XRD) using a Philips PW1729 X-ray diffractometer and Cu $K\alpha$ radiation. X-ray diffraction peak intensities were determined by a least-squares procedure. The relative intensity of representative XRD peaks was calculated using the I_x/I_t relationship, I_x being the integrated intensity for the representative peak of Li_2SiO_3 [(1 3 0)], $Li_2Si_2O_5$ [(1 1 1)], Li_4SiO_4 [(−1 1 0)], and I_t being the sum of the integrated intensity for the representative peaks of the constituent phases of the final product.

The size and morphology of the lithium metasilicate dendrites structure was studied using a FEI Tecnai G^2 TF 20 UT 200 kV transmission electron microscope (TEM). The sample was dispersed in acetone and deposited onto a hollow carbon grid, followed by acetone evaporation at room temperature in air prior to insertion in the microscope. Scanning electron microscopy (SEM) was carried out with a Leo 1550 Gemini microscope operated at a working distance of 3–4 mm and an electron acceleration voltage of 3.0 kV for imaging. Chemical composition was determined by energy dispersive X-ray spectroscopy (EDX) detectors attached to the TEM and SEM microscopes.

Thermogravimetric (TG) and differential scanning calorimetric (DSC) analysis were performed using a Netzsch STA 449C Jupiter. Approximately 10 mg of material was kept in sintered Al_2O_3 crucibles and the temperature was increased from room temperature to 700 and to 1150 °C at a heating rate of 20 °C/min. The measurements were conducted under static air and under argon flow (100 cm^3/min) conditions, respectively. In situ gas analysis was performed using a mass spectrometer (Netzsch: QMS 403 C Aëolos) through a heated transfer capillary.

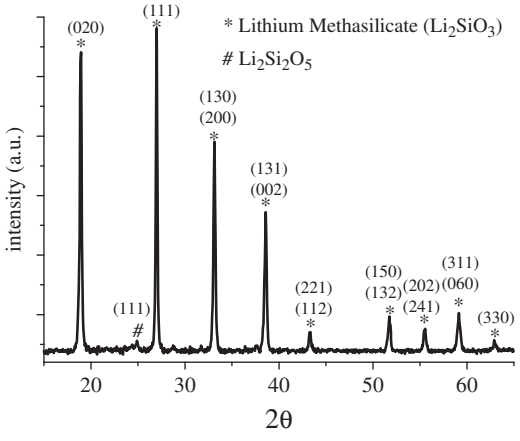

Fig. 1. XRD pattern of the Li_2SiO_3 synthesized from SBA-15 with flake morphology. Indexed planes are given in bracket. (Li_2SiO_3, JCPDS Data file: 29-0828.)

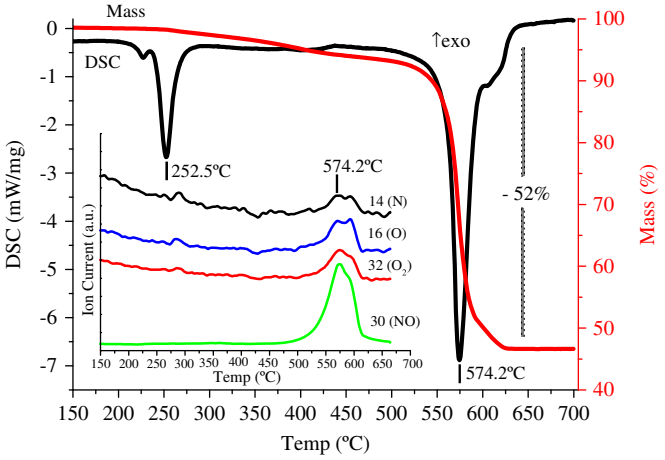

Fig. 2. TG/DSC and gas analysis (inset) curves of the synthesis reaction measured in air.

3. Results and discussion

In Fig. 1 the X-ray diffractogram of sample 1 (Table 1) is presented where the diffraction peaks of the final product are indexed to the lithium metasilicate orthorhombic structure. The final product consists of lithium metasilicate of high purity with a small amount of the side-product $Li_2Si_2O_5$. The constituent product phases and the relative intensity of representative XRD peaks (number in bracket) for these phases are shown in Table 1.

To determine the reactions occurring during thermal processing, simultaneous TG/DSC and gas analysis were carried out for the initial mixture, i.e. after step 1, and the results are presented in Fig. 2. DSC reveals two endothermic reactions between 250 and 600 °C. The first endothermic peak (252 °C) is related to the melting of $LiNO_3$ (T_m=253 °C) [26]. The endothermic peak associated with a weight loss of ~52% (w/w) at 574 °C is caused by the reaction between $LiNO_3$ and SiO_2. At the same temperature gas analysis shows the presence of NO and O_2 as products of the

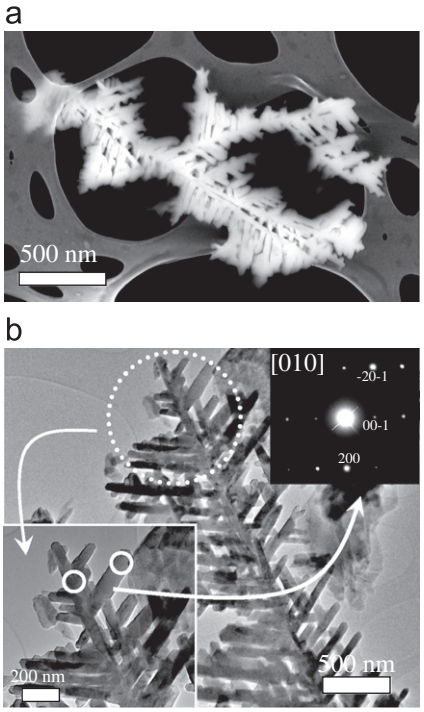

Fig. 3. SEM (a) and TEM (b) micrographs of the Li_2SiO_3 dendrite (sample 1). The corresponding ED pattern and higher resolution micrographs are shown in the insets.

reaction (Fig. 2 inset). The presence of O and N is a result from the dissociation of the NO and O_2 in the mass spectrometer.

From data obtained from DSC/TG and gas analysis a mechanism where Li_2SiO_3, NO and O_2 are products of the reaction of $LiNO_3$ and SiO_2 are proposed according to the following reaction:

$$2LiNO_3 + SiO_2 \rightarrow Li_2SiO_3 + 2NO(\uparrow) + 3/2O_2(\uparrow)$$

Also, the theoretical weight loss associated to this reaction (54% (w/w)) agrees with the weight change observed in the TG analysis (52% (w/w)).

Fig. 3 displays SEM (a) and TEM (b) micrographs of the as-prepared dendrite Li_2SiO_3 nanostructures. The dendritic morphology of Li_2SiO_3 nanostructures with a size of several microns is observed from Fig. 3(a). The typical 1-fold nanodendrite is composed of one trunk, several microns in length and some tens of nanometers in diameter, and small branches of several hundreds of nanometers in length and up to 70 nm in diameter symmetrically distributed on two sides of the trunk. The branches are all located in the same plane. All branches on one side of the trunk are parallel to each other and grow at an angle of $\sim 60^\circ$ with respect to the trunk.

In order to study the crystal structure of the obtained material, Li_2SiO_3 dendrites were characterized by TEM and selected area electron diffraction (SAED). A typical TEM micrograph of a single dendrite is shown in Fig. 3(b). The single crystal nature of the Li_2SiO_3 was confirmed by electron diffractometry by obtain identical SAED patterns from both the trunk and the branches. From SAED it is also clear that the dendritic structure grow in the $<1\,0\,0>$ direction.

In Fig. 4 the mass evolution and DSC response as a function of temperature of sample 1, i.e. the decomposition process of the dendritic structure, is shown. The sample loses mass in two steps. The first mass loss, which occurs between 180 and 450 °C, is attributed to the dehydration and dehydroxilation of the sample. The second step (between 725 and 950 °C) is attributed to lithium

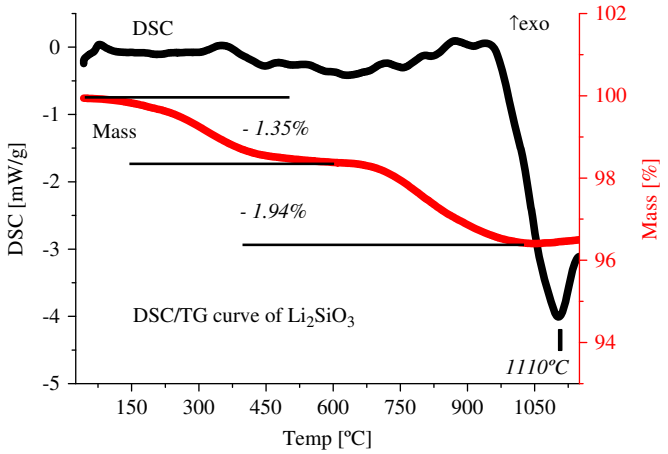

Fig. 4. TG/DSC curves of the nanodendrite Li_2SiO_3 powder measured under argon flow.

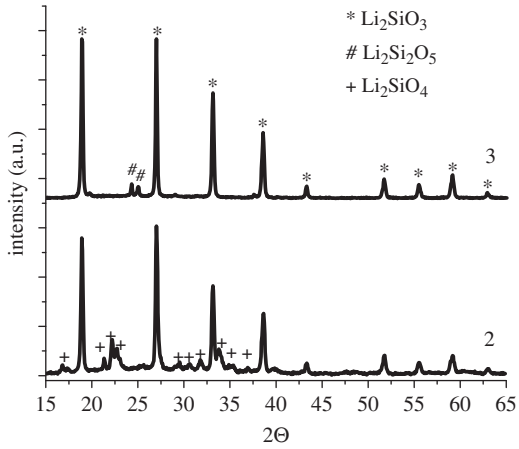

Fig. 5. XRD patterns of synthesized lithium silicates products obtained. (2) from SBA-15 (particles) and (3) from SBA-16 (hollow spheres). (JCPDS Data files: Li_2SiO_3, 29-0828; $Li_2Si_2O_5$, 30-0767; Li_4SiO_4, 37-1472.)

sublimation since it has been reported to occur at temperature around 800 °C [27]. The lithium evaporates then as Li_2O gas. The endothermic reaction observed in the DSC-response at 1100 °C corresponds to melting of Li_2SiO_3. This is in accord with the phase diagrams of the Li_2O–SiO_2 system [28], which indicates a melting temperature of 1033 °C and keeping in mind that the DSC-response was recorded at a heating rate of 20 °C/min.

In order to determine the role of the mesoporous structure in the Li_2SiO_3 dendrite synthesis we also investigate the use of other mesoporous silica species as substrate. The source of silica to sample 2 was SBA-15 (hexagonally ordered tubular pore structure) with a pore diameter of ~5.0 nm and for the sample 3, SBA-16 (spherically shaped pore cages arranged in a cubic lattice) with a pore diameter of ~7.8 nm. The pore arrangement, pore size and surface area of each sample are shown in Table 1.

Fig. 5 shows X-ray diffractograms of samples 2 and 3. In both samples the presence of lithium metasilicate is apparent. However, the presence of side-products is more notable compared to sample 1. In sample 2 the side-product is Li_4SiO_4, while sample 3 shows the presence of $Li_2Si_2O_5$. Table 1 shows the relative intensity of representative XRD peaks for these phases.

Fig. 6 shows TEM micrographs of the morphology of the compounds synthesized in samples 2 and 3. In these samples, Li_2SiO_3 (Fig. 6(a)) particles as well as $Li_2Si_2O_5$ and Li_4SiO_4 (Fig. 6(b)) compounds show a spherical shape opposite of the

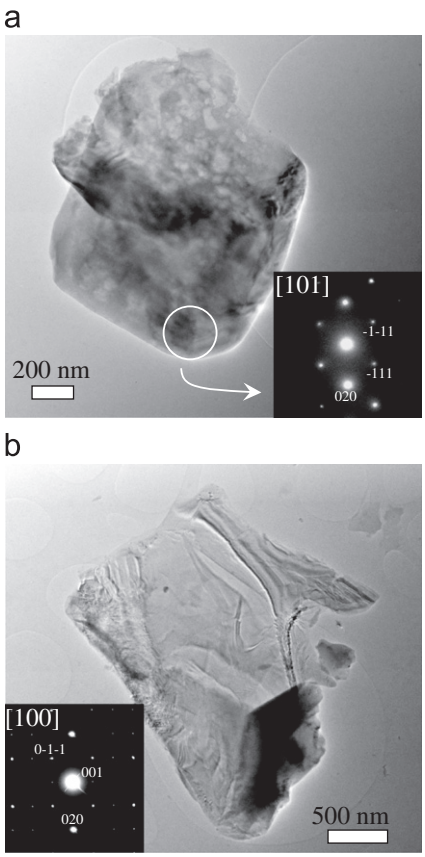

Fig. 6. TEM micrograph of the (a) Li_2SiO_3 (sample 4) and (b) $Li_2Si_2O_5$ (sample 3). The corresponding ED patterns are shown in the insets.

dendritic growth shown in sample 1 (Fig. 3). The micrograph shown in Fig. 6(b) correspondence to $Li_2Si_2O_5$ (sample 3) and SAED is shown in the inset. The Li_2SiO_3 SAED pattern can be indexed along the [1 0 1] zone axis (Fig. 6(a)), and in the Fig. 6(b) the SAED pattern of $Li_2Si_2O_5$ was indexed along the [1 0 0] zone axis.

In general, crystal growth behavior and resulting morphology are governed by a range of parameters such as the degree of supersaturation, diffusion of reacting species to the surface of the crystals, surface and interfacial energy, and the structural anisotropy of the crystals [29]. It is well established that non-equilibrium conditions at the liquid-solid interface [30], and physical processes such as thermal diffusion and solute diffusion [31] provide a driving force for the dendritic growth.

The results reported in this paper should have implications for dendritic crystal growth. The pore size of the mesoporous structure was an important factor that affected the final product's morphology. Regarding the growth process, $LiNO_3$ diffusion in the mesoporous channels plays a key role in the formation of these morphologies. The larger pore size in sample 1 promotes the diffusion of Li ions providing sufficient means for the necessary solute concentration gradient. In the case of sample 2 with narrower pore channels the smaller pore size obstructs the diffusion of the species in the pore. This fact gives rise different concentration distributions such that the growth conditions for the metal silicate will differ.

Under constant synthesis parameters, the non-equilibrium concentration distribution of $LiNO_3$ at the liquid–solid interface determines the morphology of the grown nanoarrays. Therefore, such non-equilibrium concentration at the liquid-solid interface is affected by varying the pore size. In other words, the pore size-related nature of the morphology presented in Figs. 3 and 6 results from the pore size-dependent diffusion rate of $LiNO_3$. The pore size in sample 1 is apparently large enough to avoid blocking of the pore entrance and allow for sufficient diffusion of all needed chemicals inside the mesoporous framework. For the sample with smaller pores the diffusion is limited by the effectively higher molecular friction coefficient caused by a higher surface to volume ratio in the porous framework. In addition, precipitation of solid products inside the pores will more severely obstruct the necessary diffusion inside the silica pore.

Based on these results we propose that the reaction when dendrites are formed in sample 1 starts inside the pores and grows through the mesoporous particle as it consumes the silica framework, i.e. a growth from inside and out. In the other cases with smaller pore sizes the rate at which the reactants are supplied inside the porous framework is not sufficient to have the dendritic growth to be dominating. Instead the dominating reaction site is the outside surface of the porous silica particle resulting in a growth that could be described as growth from outside and in. The resulting morphology is then spherical shaped particles

In relation with other approaches and methods such as solid-state reactions, precipitation, and sol–gel a relatively high-purity (97%) lithium metasilicate has been obtained here [32,33]. The high purity is a result of the mechanism, in which the side products of the reaction are gases. In comparison with other reports [33,34] where amorphous silica was used as the silica source, the pore arrangement present in the mesoporous structure has proven to form an adequate environment for the non-equilibrium condition needed for the synthesis of dendritic morphologies.

4. Conclusions

In summary, we have presented a simple template-based method for preparing unusual 2-D lithium metasilicate (Li_2SiO_3) dendritic nanostructures. It was found that the pore size of the SiO_2-based mesoporous plays an important role in the formation of well-defined Li_2SiO_3 dendritic nanostructure. The high purity of the final Li_2SiO_3 is explained by the reaction mechanism proposed, where the side product of the Li_2SiO_3 synthesis are gases (NO and O_2). This templated synthesis method provides a new route for direct growth of dendritic nanostructures.

References

[1] A.P. Alivisatos, Journal of Physical Chemistry 100 (1996) 13226–13239.
[2] M.A. El-Sayed, Accounts of Chemical Research 34 (2001) 257.
[3] K.A. Dick, K. Deppert, M.W. Larsson, T. Martensson, W. Seifert, L.R. Wallenberg, L. Samuelson, Nature Materials 3 (2004) 380–384.
[4] J.Y. Lao, J.G. Wen, Z.F. Ren, Nano Letters 2 (2002) 1287–1291.
[5] E. Hosono, T. Kudo, I. Honma, H. Matsuda, H.S. Zhou, Nano Letters 9 (2009) 1045–1051.
[6] K. Shankar, J. Bandara, M. Paulose, H. Wietasch, O.K. Varghese, G.K. Mor, T.J. LaTempa, M. Thelakkat, C.A. Grimes, Nano Letters 8 (2008) 1654–1659.
[7] L. Samuelson, Materials Today 6 (2003) 22–31.
[8] K.F. Hesse, Acta Crystallographica Section B—Structural Science 33 (1977) 901–902.
[9] A.S. Bhalla, L.E. Cross, R.E. Newnham, Journal of Crystal Growth 46 (1979) 262–264.
[10] K. Ben Saad, H. Hamzaoui, A. Labidi, B. Bessais, Applied Surface Science 254 (2008) 3955–3958.
[11] R.X. Li, Y. Yamaguchi, Y. Shu, T. Qing, T. Sato, Solid State Ionics 172 (2004) 235–238.
[12] P.X. Zhu, M. Teranishi, J.H. Xiang, Y. Masuda, W.S. Seo, K. Koumoto, Thin Solid Films 473 (2005) 351–356.
[13] A. Klix, Y. Verzilov, K. Ochiai, T. Nishitani, A. Takahashi, Fusion Engineering and Design 72 (2005) 327–337.
[14] J. Charpin, F. Botter, M. Briec, B. Rasneur, E. Roth, N. Roux, J. Sannier, Fusion Engineering and Design 8 (1989) 407–413.
[15] A.R. Raffray, M.C. Billone, G. Federici, S. Tanaka, Fusion Engineering and Design 28 (1995) 240–251.
[16] J. Jimenezbecerril, P. Bosch, S. Bulbulian, Journal of Nuclear Materials 185 (1991) 304–307.

[17] C.W. Turner, B.C. Clatworthy, A.Y.H. Gin, Pittsburgs, 1987.
[18] H.C. Liao, Y. Sun, G.X. Sun, Materials Science and Engineering a-Structural Materials Properties Microstructure and Processing 335 (2002) 62–66.
[19] D. Cruz, S. Bulbulian, Journal of the American Ceramic Society 88 (2005) 1720–1724.
[20] C.E. Johnson, K.R. Kummerer, E. Roth, Journal of Nuclear Materials 155 (1988) 188–201.
[21] D. Vollath, H. Wedemeyer, E. Gunther, Journal of Nuclear Materials 133 (1985) 221–225.
[22] D.I.H. Atkinson, P.W. McMillan, Journal of Materials Science 12 (1977) 443–450.
[23] B.R. Durschang, G. Carl, C. Russel, K. Marchetti, E. Roeder, Glastechnische Berichte—Glass Science and Technology 67 (1994) 171–177.
[24] M.A. Ballem, J.M. Córdoba, M. Odén, Microporous and Mesoporous Materials 129 (2010) 106–111.
[25] E.M. Johansson, J.M. Cordoba, M. Oden, Materials Letters 63 (2009) 2129–2131.
[26] CRC, Taylor and Francis Group LLC, London 90th edition (2009–2010).
[27] H. Pfeiffer, K.M. Knowles, Journal of the European Ceramic Society 24 (2004) 2433–2443.
[28] F.C. Kracek, The Journal of the Pysical Chemistry 34 (1930) 2645–2650.
[29] J. Nittmann, H.E. Stanley, Nature 321 (1986) 663–668.
[30] R. Trivedi, W. Kurz, International Materials Reviews 39 (1994) 49–74.
[31] B. Cantor, A. Vogel, Journal of Crystal Growth 41 (1977) 109–123.
[32] H. Pfeiffer, P. Bosch, S. Bulbulian, Journal of Nuclear Materials 257 (1998) 309–317.
[33] T. Tang, Z. Zhang, J.B. Meng, D.L. Luo, Fusion Engineering and Design 84 (2009) 2124–2130.
[34] M.K. Brun, A.S. Bhalla, K.E. Spear, L.E. Cross, R.S. Berger, Journal of Crystal Growth 47 (1979) 335–340.